Hindawi
International Journal of Aerospace Engineering
Volume 2023, Article ID 8827361, 8 pages
https://doi.org/10.1155/2023/8827361

Research Article

Design of the Space Camera Protection System during Launch Process

Siyu Wang, Haiying Tian, and Changxiang Yan

Changchun Institute of Optics, Fine Mechanics and Physics, Chinese Academy of Sciences, Changchun 130033, China

Correspondence should be addressed to Siyu Wang; cas_yu@126.com

Received 7 June 2023; Revised 9 September 2023; Accepted 26 September 2023; Published 12 October 2023

Academic Editor: Zhiguang Song

In order to improve the safety and reliability and maintain the stability of imaging quality when a space camera with a cargo spaceship is launched, a protection system for the space camera is designed. Firstly, according to the mechanical properties of the space camera, a working principle of the protection system is elaborated, and a model of the system is proposed. Secondly, a protective cover and a vibration isolation block are designed on the basis of shape, size, and requirements of the space camera. Thirdly, based on the finite element mesh, static and sinusoidal vibration simulation calculations of the space camera and its protection system are carried out. Finally, the protection system is validated after mechanical experiment. The results reveal that the three directional fundamental frequencies of space camera are 43.39 Hz, 26.74 Hz, and 22.83 Hz, respectively, and the maximum response of sinusoidal vibration acceleration is 17.02 g, which is amplified by 3.4 times. The image quality of the space camera lens is consistent before and after the test, which satisfies the requirement of the cargo ship.

1. Introduction

Various space science research and technical experiment verification will be gradually realized with China's space station continuous construction. The space camera will be installed on the external facade of the experimental module after docking with the space station. Then, experiments on large field view spatial imaging technology will be conducted. It faces two problems during the launching process. The first problem is that the rocket generates sinusoidal and random vibration during the launching process, which causes impact and vibration due to the influence of external air flow. Due to complex structure, large size of the space camera, loading of precision components, and rotating parts, high requirements are put forward for its structural strength, stiffness, and dynamic environment adaptability. However, the structural strength of the camera body is limited. The second problem is that the space camera cannot be carried up by satellite with conventional loads. It needs to be loaded in cargo bags and transported with other loads and docked with the space station for transfer. As the direct coverage of the freight package will squeeze the rotating parts of the camera, the original thermal coating will be damaged, and the normal experiment and use of the camera will be affected. Therefore, it is another important problem to increase the overall strength and stiffness of the camera and avoid the coating that touches the important coating of the camera.

In recent years, the main methods to suppress the impact of vibration are as follows: for instance, the vibration isolation method is used to isolate the space camera from the rocket to reduce the impact of vibration. The passive vibration isolation method is widely used because of its compact structure, small size, and strong reliability [1–3]. Wang et al. adopted passive local vibration isolation technology to design the impact resistance of space optical load detector [4]. Zhang et al. designed a passive vibration isolation system for the task requirements of micro-nano-space camera [5]. Chen et al. established a double passive vibration isolation system, which makes the mechanical structure simpler and more effective for vibration attenuation [6]. The other method is to increase the strength and stiffness of the structure by adding ribs or shells to protect the load and reduce the impact of vibration. Tan et al. combined the satellite's

own structure. The method of adding stiffened rib plates was proposed to solve the problem of excessive response [7]. Benton made a preliminary study on the Mars probe through the modular design method of spacecraft and cargo lander and increased the shell to improve the reliability [8]. However, there is little literature on the improvement of load strength and upgoing coverage of cargo ships.

This paper takes the practical problems of aerospace engineering as the research source, is aimed at improving the reliability of the space camera going up with the cargo ship, and takes avoiding the impact of vibration and covering touch as the constraint condition, to carry out the research on the space camera ascending protective cover. First of all, according to the mechanical characteristics of the space camera, the working principle of the protection system is described, and the protection system model is proposed. Next, design the size, material, and shape of the protection system according to the shape, size, and requirements of the space camera. Then, based on the finite element mesh division, the static and sinusoidal vibration simulation of the space camera and the protection system are carried out. Ultimately, the protection system is verified by mechanical experiments and simulation analysis.

2. Principle of the Protection System

2.1. Mechanical Properties of the Space Camera. The model of the space camera is shown in Figure 1, with a size of 585 mm × 428 mm × 439 mm. The space camera is mainly composed of optical imaging system, mechanical motion system, structural support system, and control system. Its motion and support system is made of titanium alloy material, which weights 67 kilograms. It can be rotated on the horizontal axis and the elevation axis to achieve the imaging function of large field of view space targets. The space camera needs to be isolated from the spacecraft because of its high external stiffness and contains fragile components inside.

2.2. Characteristics of the Space Camera Load Package. Loading package of space camera which size is 620 mm × 500 mm × 620 mm. Obviously, it is larger than the space camera, so the interior of the loading package can be designed to be filled with vibration isolation blocks. As the rocket needs to be well fixed during launch, the camera needs to be bundled and tightened. The bundling process will crush and damage the space camera, so the camera shall be separated from the loading package by a protective cover. Therefore, the space phase needs to take protective system measures to isolate the camera from the external mechanics and reduce vibration.

2.3. Working Principle of the Protection System. The basic working principle of the protection system is when the space camera receives the binding force, the protective cover has enough stiffness to isolate the space camera from the outside world and avoid being touched or squeezed, and when the rocket is subject to vibration during launch, part of the energy received will be stored in the protection system, resulting in the deformation of the protection system. The deformation

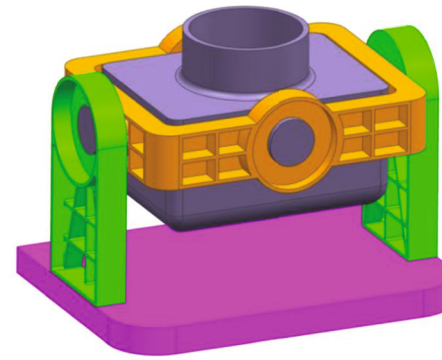

Figure 1: Model of the space camera.

can be released with the fundamental frequency and high frequency cycle, reducing the deformation displacement of the space camera and realizing the buffering effect on vibration. Therefore, the protection system needs to ensure the design requirements of sufficient stiffness and flexibility. In addition, due to the limited cargo space load, the weight of the protection system needs to be controlled below 205 kilograms, and lightweight optimization design needs to be carried out.

Since the mass of the cargo ship M is far exceeds than the mass of the space camera m, the mechanical model of the protection system can be obtained according to the simplified mechanical model of the space camera which shown in Figure 2.

The mechanical equation of the space camera can be simplified as follows [9–13]:

$$m\ddot{x}_1 + c(\dot{x}_1 - \dot{x}_2) + k(x_1 - x_2) = u \tag{1}$$

where M is the mass of rocket and the cargo ship, m is the mass of the space camera, x_1 is the amplitude of the spacecraft, x_2 is the amplitude of the space camera system, c is the damping coefficient of the vibration isolator, k is the stiffness of the protective cover, and u is the forced vibration of the spacecraft [10, 12, 13].

The damping ratio is

$$\zeta = \frac{c}{2\sqrt{kM}}. \tag{2}$$

The frequency ratio is

$$\lambda = \frac{\omega}{\sqrt{k/M}}. \tag{3}$$

Transmissibility is

$$T = \frac{|x_1|}{|x_2|} = \frac{1}{\sqrt{(1-\lambda^2) + 4\zeta^2\lambda^2}}. \tag{4}$$

Calculate the characteristic solution according to formula (4), as shown in Figure 3. When the frequency ratio λ is greater than 1.414, the transmissibility of the protection system is less than 1; this conclusion is not affected by the

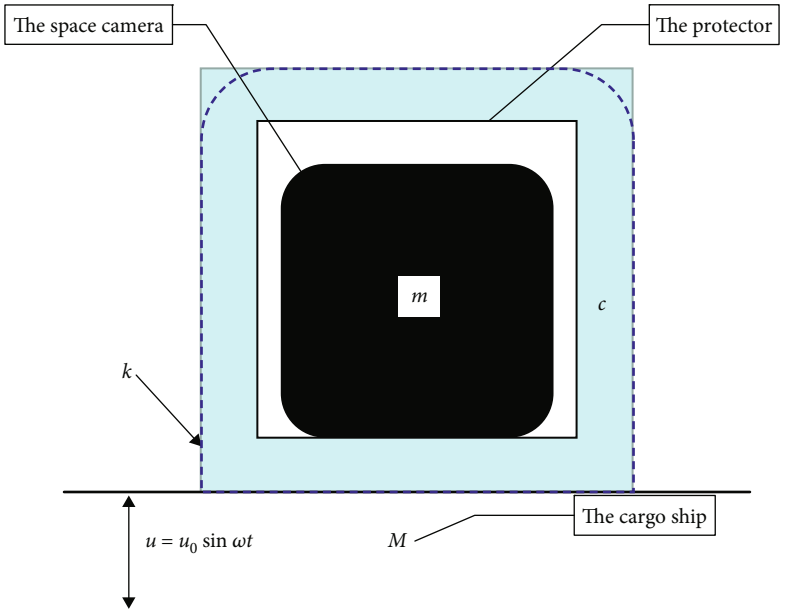

Figure 2: Simplified mechanical model of space camera.

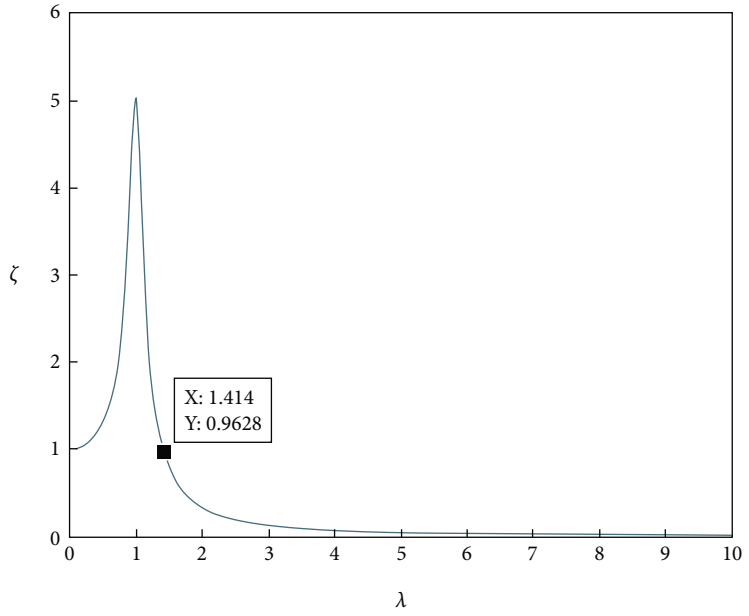

Figure 3: Transmissibility and frequency ratio.

change in damping ratio ζ. The fundamental frequency of the rocket cargo ships is 15 Hz. Therefore, it should be ensured that the fundamental frequency of the space camera is greater than 21.21 Hz when adding a protection system.

3. Design of the Protection System

3.1. Structure of the Protector. A protector can provide protection and support for the space camera. The protector is composed of a box, a cover, and Velcro. The box and cover are made of high-strength aluminum alloy, and the Velcro is made of nylon, as shown in Figure 4.

The size of the box is 640 mm × 640 mm × 460 mm, its rigidity is strengthened with ribs, and its weight is reduced with weight reduction holes. The weight of the box is 16.8 kilograms. The size of the cover is 640 mm × 640 mm × 50 mm, and the position of cargo grid buckle and handles of camera are reserved. The cover is the same as the box, strengthening its stiffness through ribs and reducing its weight through weight reduction holes. The weight of cover is 5.2 kilograms.

The installation steps of the protection system are to put the camera into the box by two handrails first, then use 10 screws to pass through the bottom of the box, and secure it to the threaded holes at the bottom of the space camera. At this point, the space camera is already packed in the

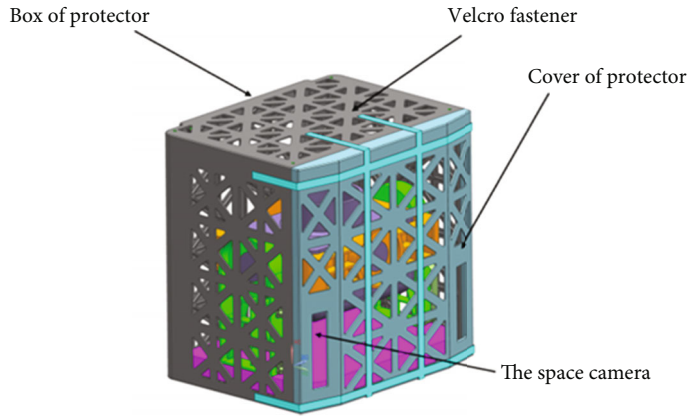

Figure 4: Protector structure of the space camera.

box. Then, fasten the cover and tightly attach the Velcro fastener, so that the cover and the box are assembled together as a whole system. Finally, install four lifting rings on the top of the system, which can be used for transportation and packaging.

3.2. The Device of Buffer Protection. The device of buffer protection is shown in Figure 5, which is collaged by eight pieces of shaped and placed into the cargo for loading. Polyurethane foam material is selected as the shaped protective part which is covered with antistatic cloth on the surface. It is a high molecular polymer foamed with isocyanate and polyether as the main raw materials, with heat preservation and buffering functions [14–16]. The total weight of the device of buffer protection is about 8.2 kilograms.

When the space camera is impacted and vibrated, the polymer inside the shaped protective part will produce relative slip, which will consume part of its energy through intermolecular friction, so as to achieve the purpose of vibration isolation. Consequently, the shaped protective part will be deformed and released slowly, with the vibration cycle of the space camera and the protector, to achieve the vibration isolation effect.

4. Simulation

4.1. Line Static Structural Analysis. The protector is placed in the direction of the ground during packaging and placed in the upward direction during transportation. Considering the different directions with packaging and transport of the space camera, static analysis of the protective system needs to be conducted separately for different scenarios. The material parameters of protection system are shown in Table 1.

The grid convergence test is shown in Table 2. The density of the mesh is doubled, and the maximum relative error of the deformation is 0.74%; therefore, it can be considered that the finite element model mesh converges.

The static analysis of the protector during packaging is shown in Figure 6. Maximum deformation of the packaging process analysis result is 5.5×10^{-2} mm. The static analysis of the protector during transportation is shown in Figure 7. Maximum deformation of the transportation analysis result is 3.4×10^{-2} mm.

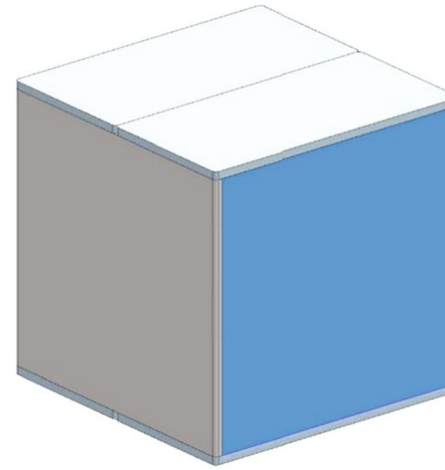

Figure 5: The device of buffer protection.

Table 1: The material parameters of protection system.

Property	Value	Unit
Density	2.8×10^{3}	kg/m^3
Coefficient of thermal expansion	2.3×10^{5}	1/°C
Young's modulus	7.1×10^{10}	Pa
Poisson's ratio	3.3×10^{-1}	
Tensile yield strength	2.8×10^{8}	Pa

Table 2: The grid convergence test.

Mesh size	Transportation	Packaging
5 mm	3.4427×10^{-2}	5.7565×10^{-2}
2.5 mm	3.3975×10^{-2}	5.5706×10^{-2}
1.25 mm	3.3722×10^{-2}	5.5292×10^{-2}
Relative error	0.74%	0.72%

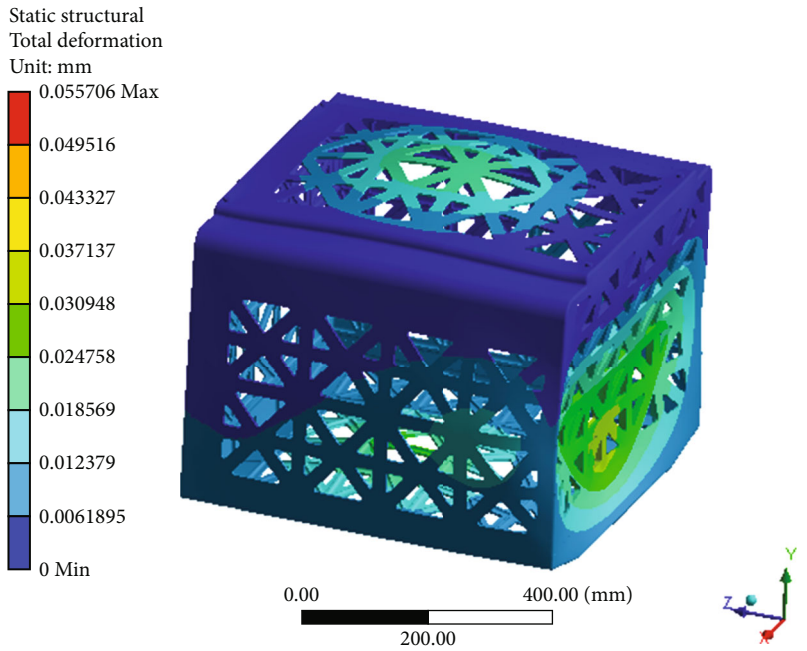

Figure 6: Static analysis of packaging.

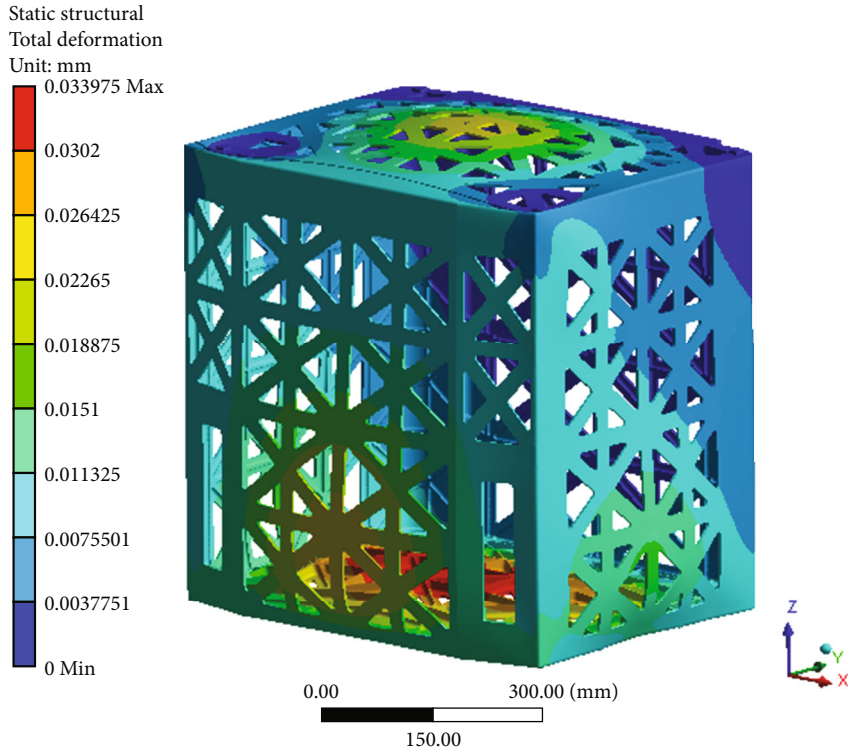

Figure 7: Static analysis of transportation.

4.2. Dynamic Analysis

4.2.1. Modal Calculation. In order to obtain the dynamic characteristics of the protector and the space camera, the modal calculation is carried out first. Calculation results of the first 4 modes of the space camera and protection system are shown in Table 3.

4.2.2. Sinusoidal Vibration Analysis. The equation of motion for sinusoidal vibration is [17]

$$\left(-\omega^2[M] + i\omega[C] + [K]\right)\left(\{\phi_1\} + i\{\phi_2\}\right) = \left(\{F_1\} + i\{F_2\}\right). \quad (5)$$

In this formula, the stiffness matrix is $[K]$, the mass

Table 3: Calculation results of the first 4 modes.

Modal order	Frequency
1	24.2 Hz
2	25.1 Hz
3	45.5 Hz
4	48.0 Hz

Table 4: Sinusoidal vibration test conditions.

Frequency (Hz)	0-17	17-60	60-100
Target peak(g)	2.2	5.8	2.5
Load scan rate		2 oct/min	
Load scan direction		X, Y, Z	

Table 5: Acceleration response of sinusoidal vibration in three directions.

Direction	X	Y	Z
Acceleration response	17.4 g	23.6 g	24.5 g
Acceleration magnification	2.9	3.93	4.1

Table 6: Identification load of the three direction sinusoidal vibration screws (from Supplementary Table 1–3).

Direction	F_1 (N)	F_2F_3 (N)	M_1M_2 (N·M)	M_3 (N·M)
X	226.9	43.9	116.2	32.1
Y	221.0	39.2	110.0	26.8
Z	214.1	74.7	291.2	40.8

Table 7: Safety margin of sinusoidal vibration screw in three directions (from Supplementary Table 1–3).

Direction	F_1	F_2F_3	M_1M_2	M_3
X	0.6	16.0	2.6	16
Y	0.7	12.1	3.0	23.1
Z	0.65	12.0	0.9	9.4

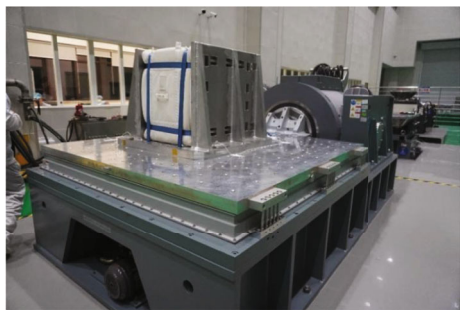

Figure 8: Test site status.

Table 8: Sweep test data in three directions (from Supplementary Table 4).

Direction	Fundamental frequency before vibration	Fundamental frequency after vibration
X	42.72 Hz	43.39 Hz
Y	30.43 Hz	26.74 Hz
Z	21.24 Hz	22.83 Hz

matrix is $[M]$, the damping is $[C]$, and the abbreviated load is $[F]$. Sinusoidal vibration analysis is a linear analysis where any nonlinear features will be ignored. We use the modal superposition method to solve the response equation.

The sinusoidal vibration load conditions are shown in Table 4.

The acceleration response of simulated sinusoidal vibration in X, Y, and Z directions is shown in Table 5.

It can be seen that the response of Z direction sinusoidal vibration is large, the maximum acceleration is about 24.5 g, and the maximum magnification is 4.1 times. Since the camera is connected with the protective hood through the bottom screw, the stress of each screw is concerned, and the identification load is calculated according to the specific structure of the screw and the stress value of the connecting hole screw. Table 6 shows the load of X, Y, and Z direction sine vibration camera base screws. Table 7 shows the safety margin of sinusoidal vibration screw in three directions.

The data in Table 6 is from Supplementary Tables 1–3. Modifications have been made to the original table to improve the readability of the article.

The data in Table 7 is from Supplementary Tables 1–3. Modifications have been made to the original table to improve the readability of the article.

5. Experimental Verification

In order to verify the protection and mechanical vibration isolation effect of the protection system, mechanical vibration experiments were carried out on the space camera. During the vibration test, the product is connected to the protective hood at the installation base by screws. The protective hood is placed in the box and tied to the tooling by straps. The placement of the protection system in the experiment is shown in Figure 8.

5.1. Sweep Test. Table 8 shows the sweep test data in three directions.

The data in Table 8 is from Supplementary Tables 4. Modifications have been made to the original table to improve the readability of the article.

The change rate of fundamental frequency before and after the X direction test is 1.6%. The change rate of fundamental frequency before and after the Y direction test is 12.1%. The change rate of fundamental frequency before and after the Z direction test is 7.5%. After the test, the state of the space camera is normal, indicating that the structural performance is stable.

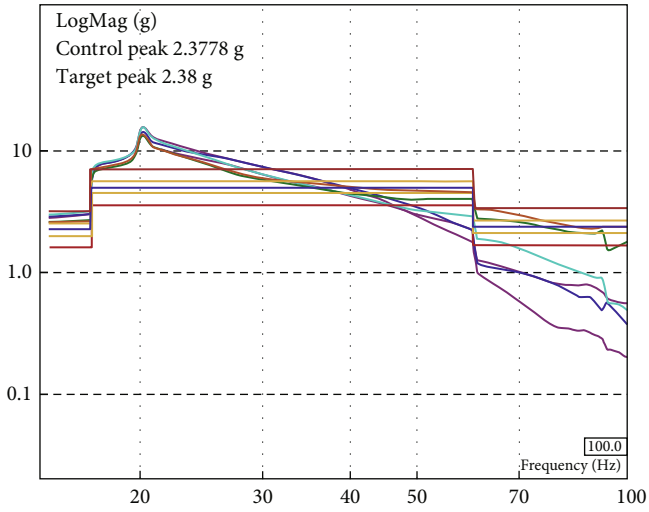

Figure 9: Sinusoidal vibration test curve in X direction.

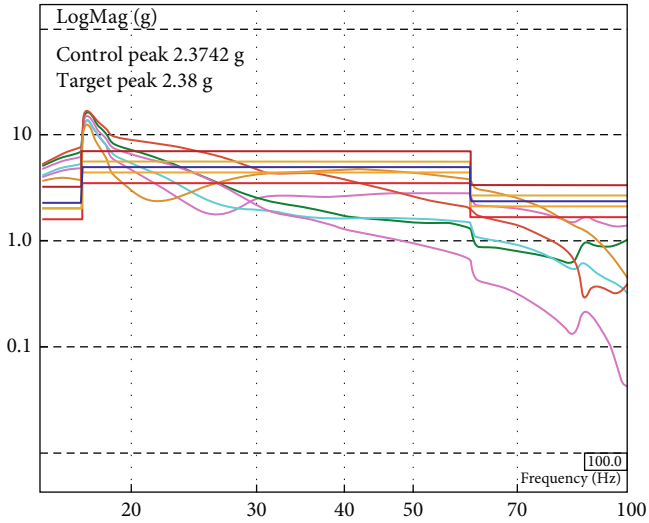

Figure 10: Sinusoidal vibration test curve in Y direction.

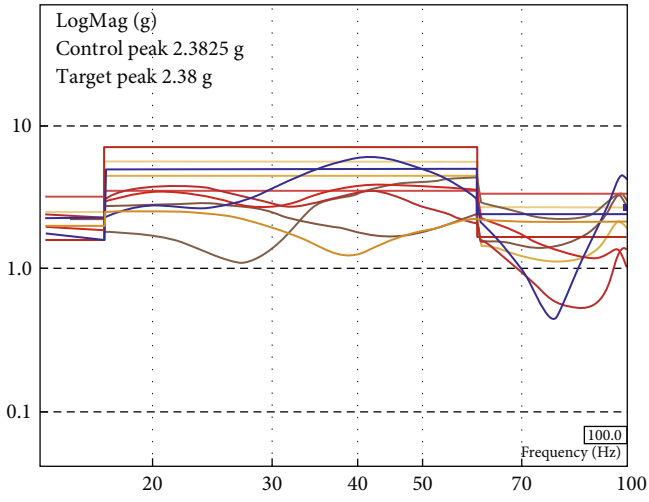

Figure 11: Sinusoidal vibration test curve in Z direction.

Table 9: Statistics of random vibration test results.

Direction	Root mean square acceleration (g)
X	42.72 Hz
Y	30.43 Hz
Z	21.24 Hz

5.2. Sinusoidal Vibration Test. Figure 9 shows the sinusoidal vibration test curve in X direction.

Sinusoidal vibration test curve in Y direction is shown in Figure 10.

Sinusoidal vibration test curve in Z direction is shown in Figure 11.

As can be seen from the figure, the maximum response of sinusoidal vibration acceleration is 17.02 g, which is amplified 3.4 times.

5.3. Random Vibration Test. Table 9 shows the statistics of root mean square acceleration results of random vibration test.

5.4. Performance Detection. Parallel optical tubes were used to detect the star image of the optical system before and after the mechanical test to determine whether the image quality deteriorated after the mechanical test. Before mechanical test, the energy concentration in star point 3×3 pixel is 0.65. After mechanical vibration test, the energy concentration in 3×3 pixels is 0.74. There is no significant asymmetric aberration such as coma and astigmatism in the image spot.

6. Conclusion

According to the safety and reliability requirements of the space camera during launch process, this paper proposes a protection system and introduces the structure and principle of the protection system during launch process. First, according to the shape, size, and requirements of the space camera, the protective cover and vibration isolation block are preliminarily designed. Then, the protection system is simulated and analyzed. Finally, the protection system is simulated and verified by mechanical experiments. This test results show that the fundamental frequencies in three directions are 43.39 Hz, 26.74 Hz, and 22.83 Hz, respectively. The maximum response of sinusoidal vibration acceleration is 17.02 g, and the amplification is 3.4 times. Before and after the vibration test, the sweep curves of all effective measuring points are consistent, the image quality of the lens is consistent before and after the test, and the lens accuracy does not decline, indicating that the space camera protection system during launch process proposed in this paper is feasible and effective.

Data Availability

The data used to support the findings of this study are included within the supplementary information file(s).

Conflicts of Interest

The authors declare that they have no conflicts of interest.

Acknowledgments

This research was funded by the National Natural Science Foundation of China (NSFC) under Grant 61627819, Grant 61727818, Grant 6187030909, Grant 61875192, and Grant 62275114; in part by the HY-Multiangle Polarizing Spectral Camera; in part by the K.C. Wong Education Foundation; in part by the High-Altitude Large UAV Airborne Visible Infrared Spectral Imager Procurement Project under Grant 21540; and in part by the National Science Fund for Distinguished Young Scholars under Grant 62105331.

Supplementary Materials

The name of the first supplementary document is Supplementary Table 1, which identifies the load and safety margin for sinusoidal vibration in X direction. The name of the second supplementary document is Supplementary Table 2, which identifies the load and safety margin for sinusoidal vibration in the Y direction. The name of the third supplementary document is Supplementary Table 3, which is the identification load and safety margin of Z direction sinusoidal vibration. Supplementary Tables 1, 2, and 3 can correspond to Tables 6 and 7 in the manuscript. The name of the fourth supplementary document is Supplementary Table 4, which represents scanning test data from three directions and can correspond to Table 8 in the manuscript. The fifth supplementary material is the calculation program, which can calculate the identification load and safety margin by inputting radial force, axial force, or bending moment. *(Supplementary Materials)*

References

[1] S. C. Kwon, M. S. Jo, and H. U. Oh, "Experimental validation of fly-wheel passive launch and on-orbit vibration isolation system by using a superelastic SMA mesh washer isolator," *International Journal of Aerospace Engineering*, vol. 2017, no. 2, Article ID 5496053, pp. 1–16, 2017.

[2] S. D. Miller, E. Swenson, R. G. Cobb, and J. Black, *Investigation of a Movel Compact Vibtrtion Isolation System for Space Applications*, Air Force Insitute of technology, 2010.

[3] A. Coronado, M. A. Trindade, and R. Sampaio, "Frequency-dependent viscoelastic models for passive vibration isolation systems," *Shock and Vibration*, vol. 9, no. 4-5, p. 264, 2002.

[4] Z. S. Wang, W. U. Qing-Wen, Q. F. Guo, L. Guo, F. Jiang, and G. Q. Wang, "Design of anti-shock vibration isolation for detector module of space optics load," *Optics and Precision Engineering*, vol. 25, no. 8, pp. 2098–2105, 2017.

[5] L. Zhang, T. L. Wang, X. Y. Zheng, Y. Zhao, and F. Zhang, "Design of a passive vibration isolation system for micro-nano space camera," *Chinese Journal of Scientific Instrument*, vol. 42, no. 2, pp. 18–25, 2021.

[6] S. Chen, M. Xuan, J. Xin et al., "Design and experiment of dual micro-vibration isolation system for optical satellite flywheel," *International Journal of Mechanical Sciences*, vol. 179, no. 1, article 105592, 2020.

[7] L. Tan, D. Wang, L. Kong, Y. Yan, and L. Li, "Suppression of random vibration response of optical satellite by matching honeycomb stiffened plates' structural parameters," *Optics and Precision Engineering*, vol. 24, no. 2, pp. 372–380, 2016.

[8] M. G. Benton, "spaceship discovery's crew and cargo lander module designs for human exploration of Mars," *AIP Conference Proceedings*, vol. 969, no. 1, pp. 898–907, 2008.

[9] J. Lin, J. Tian, M. Lu, T. Ran, and J. Zhou, "Modeling and experimental analysis on the effect of carrier aircraft vibration on the imaging quality of an aspherical aerial camera," *Optik*, vol. 232, article 166571, 2021.

[10] I. Kajiwara, S. Kitabatake, N. Hosoya, and S. Maeda, "Design of dielectric elastomer actuators for vibration control at high frequencies," *International Journal of Mechanical Sciences*, vol. 157–158, pp. 849–857, 2019.

[11] L. Yingchao and Z. Yuanjian, "Design of long focal length refractive aerial camera optical system," in *2011 International Conference on Electrical and Control Engineering*, pp. 3886–3889, Yichang, China, 2011.

[12] G. W. Zhao, D. Y. Li, and C. Yong, "Dynamic stiffness and vibration reduction efficiency of metal rubber," *Journal of Vibration and Shock*, vol. 33, no. 22, pp. 193–197, 2014.

[13] S. Honda, I. Kajiwara, and Y. Narita, "Multidisciplinary design optimization for vibration control of smart laminated composite structures," *Journal of Intelligent Material Systems and Structures*, vol. 22, no. 13, pp. 1419–1430, 2011.

[14] C.-S. Ha, "Thermal properties and sound-damping characteristics of polyurethane nanocomposite foams," *Journal of Adhesion and Interface*, vol. 11, pp. 3–8, 2010.

[15] Y. Jianmin and Z. Junhua, "Synthesis of damping semi-rigid polyurethane foam and its properties," *Polymer Materials Science & Engineering*, vol. 33, no. 7, pp. 94–98, 2017.

[16] P. Srb and R. Martonka, "Mechanical properties of polyurethane foam in different climate conditions," in *Modern Methods of Construction Design*, Lecture Notes in Mechanical Engineering, L. Ševčik, P. Lepšík, M. Petrů, I. Mašín, and R. Martonka, Eds., Springer, Cham, 2014.

[17] L. Zhao, Y. Jiang, X. Wei, L. Ma, and X. Li, "Horizontal backward launch dynamics modeling and analysis," *International Journal of Aerospace Engineering*, vol. 2019, Article ID 4098398, 9 pages, 2019.